

# Quantitative Methods for Spatially Resolved Adsorption/Desorption Measurements in Real Time by Surface Plasmon Resonance Microscopy

Jennifer S. Shumaker-Parry<sup>†</sup> and Charles T. Campbell<sup>\*</sup>

Department of Chemistry, University of Washington, Seattle, Washington 98195-1700

**A simple method for converting local reflectivity changes measured in surface plasmon resonance (SPR) microscopy to effective adlayer thicknesses and absolute surface coverages of adsorbed species is presented. For a range of high-contrast angles near the SPR resonance where the local metal surface's reflectivity changes linearly with angle, the change in reflectivity at fixed angle is proportional to the change in effective refractive index ( $\eta_{\text{eff}}$ ) near the surface. This change in  $\eta_{\text{eff}}$  can be converted to absolute adsorbate coverage using methods developed for quantitative SPR spectroscopy. A measurement of the change in reflectivity due to changes in refractive index of bulk solutions, i.e., percent reflectivity change per refractive index unit (RIU), is the only calibration required. Application of this method is demonstrated for protein adsorption onto protein/DNA arrays on gold from aqueous solution using an SPR microscope operating at 633 nm. A detection limit of 0.072% change in absolute reflectivity is found for simultaneous measurements of all 200  $\mu\text{m} \times 200 \mu\text{m}$  areas within the 24-mm<sup>2</sup> light beam with 1-s time averaging. This corresponds to a change in effective refractive index of  $1.8 \times 10^{-5}$  and a detection limit for protein adsorption of 1.2 ng/cm<sup>2</sup> ( $\sim 0.5 \mu\text{g}$  in a 200- $\mu\text{m}$  spot). The linear dynamic range is  $\Delta\eta_{\text{eff}} = \sim 0.011$  RIU or  $\sim 720 \text{ ng/cm}^2$  of adsorbed protein. Using a nearby spot as a reference channel, one can correct for instrumental drift and changes in refractive index of the solutions in the flow cell.**

Surface plasmon resonance (SPR) spectroscopy is a popular surface analysis method used to detect changes in the refractive index or thickness of an adsorbed layer on or near an SPR-active surface with high sensitivity.<sup>1–7</sup> (By “SPR spectroscopy”, we refer

here to reflectivity measurements versus both wavelength at fixed angle and angle at fixed wavelength.) Functionalization of the surface with specific binding sites creates a biosensor that can detect biomolecular interactions in real time with no labeling requirements, so SPR has become a common tool in bioanalytical chemistry.

SPR microscopy, also referred to as “imaging SPR”, provides the same advantages as SPR spectroscopy with the added feature of monitoring adsorption with a spatial resolution down to  $\sim 4 \mu\text{m}$  over a relatively large area of a sensing surface.<sup>8–14</sup> In SPR microscopy, an expanded and collimated polarized laser beam travels through a prism and reflects from a metal–dielectric interface at an angle greater than the critical angle. The reflected light intensity from the illuminated area of the surface is monitored at the specular angle by a CCD camera. Excitation of surface plasmons at the metal–dielectric interface is observed as a decrease in reflected light intensity for incident angles very near the resonance angle. The spatial contrast in an SPR microscope image comes from the heterogeneity in the complex dielectric due to differences in refractive index near the surface at different positions across the surface, which results in slight shifts in the resonance angle. This leads to changes across the surface in reflected intensity at an incident angle near the resonance angle. If an adsorbate has a refractive index different from that of the solvent, its presence on the surface can thus be detected in a spatially resolved way simply by monitoring changes in reflected light intensity.<sup>13,15–21</sup>

<sup>\*</sup> Corresponding author. E-mail: campbell@chem.washington.edu. Fax: 206-616-6250.

<sup>†</sup> Current address: Max-Planck-Institut für Polymerforschung, Ackermannweg 10, D-55128 Mainz, Germany.

- (1) Lukosz, W. *Biosens. Bioelectron.* **1991**, *6*, 215–225.
- (2) Liedberg, B.; Nylander, C.; Lundstrom, I. *Biosens. Bioelectron.* **1995**, *10*, R1–R9.
- (3) Hutchinson, A. M. *Mol. Biotechnol.* **1995**, *3*, 47–54.
- (4) Garland, P. B. *Q. Rev. Biophys.* **1996**, *29*, 91–117.
- (5) Huber, A.; Demartis, S.; Neri, D. *J. Mol. Recognit.* **1999**, *12*, 198–216.
- (6) Rabbany, S. Y.; Donner, B. L.; Ligler, F. S. *Crit. Rev. Biomed. Eng.* **1994**, *22*, 307–346.
- (7) Jonsson, U.; Malmqvist, M. In *Advances in Biosensors*; Turner, A., Ed.; JAI Press Ltd.: San Diego, 1992, 291.

- (8) Rothenhausler, B.; Knoll, W. *Nature* **1988**, *332*, 615–617.
- (9) Zizlsperger, M.; Knoll, W. *Prog. Colloid Polym. Sci.* **1998**, *109*, 244–253.
- (10) Aust, E. F.; Sawodny, M.; Ito, S.; Knoll, W. *Scanning* **1994**, *16*, 353–361.
- (11) Knoll, W. *Annu. Rev. Phys. Chem.* **1998**, *49*, 569–638.
- (12) Berger, C. E. H.; Beumer, T. A. M.; Kooyman, R. P. H.; Greve, J. *Anal. Chem.* **1998**, *70*, 703–706.
- (13) Thiel, A. J.; Frutos, A. G.; Jordan, C. E.; Corn, R. M.; Smith, L. M. *Anal. Chem.* **1997**, *69*, 4948–4956.
- (14) Lyon, L. A.; Holliway, W. D.; Natan, M. J. *Rev. Sci. Instrum.* **1999**, *70*, 2076–2081.
- (15) Li, M.; Lee, H. J.; Condon, A. E.; Corn, R. M. *Langmuir* **2002**, *18*, 805–812.
- (16) Guedon, P.; Livache, T.; Martin, F.; Lesbre, F.; Roget, A.; Bidan, G.; Levy, Y. *Anal. Chem.* **2000**, *72*, 6003–6009.
- (17) Jordan, C. E.; Corn, R. M. *Anal. Chem.* **1997**, *69*, 1449–1456.
- (18) Nelson, B. P.; Frutos, A. G.; Brockman, J. M.; Corn, R. M. *Anal. Chem.* **1999**, *71*, 3928–3934.
- (19) Nelson, B. P.; Grimsrud, T. E.; Liles, M. R.; Goodman, R. M.; Corn, R. M. *Anal. Chem.* **2001**, *73*, 1–7.
- (20) Frutos, A. G.; Brockman, J. M.; Corn, R. M. *Langmuir* **2000**, *16*, 2192–2197.

SPR microscopy has been investigated as a promising tool for simultaneously monitoring binding events across a functionalized sensor surface. By creating an array of binding sites on an SPR-active surface, DNA–DNA,<sup>13,15,16,18,22</sup> RNA–DNA,<sup>19</sup> and protein–DNA<sup>20,21,23</sup> interactions have been studied in a parallel fashion by SPR microscopy. However, no method has yet been developed for the conversion of signals in SPR microscopy to absolute adsorbate coverages (number of species per unit area).

Nelson et al.<sup>19</sup> calibrated the saturation intensity changes seen in SPR microscopy when DNA hybridizes onto a DNA-functionalized spot on a gold surface. In a separate control experiment, they adsorbed fluorescently labeled DNA onto a much larger but similarly functionalized gold surface, rinsed with HCl solution to desorb the monolayer, and measured the fluorescence signal from the rinse solution. In this way, they showed that the 0.6% reflectivity change must correspond to a saturation coverage of  $\sim 1 \times 10^{12}$  DNA/cm<sup>2</sup>. Such measurements are laborious and require the ability to functionalize a large surface area in exactly the same way as the small spots, which is not always possible. The procedure we describe below overcomes these difficulties.

Two methods for quantitative conversion of signals in SPR microscopy into absolute adsorbate coverages can be imagined based on what has been done in SPR spectroscopy. These methods both rely on measuring the full curve of reflected light intensity versus angle of incidence (always detecting at the specular angle, where the light intensity is by far the greatest). The resulting angular spectrum shows a sharp decrease in reflected light intensity at the SPR angle. This loss of energy is due to resonance excitation of the surface plasmons at the gold film–solution interface by incident photons. The exact angle where this occurs depends on the dielectric properties of the layer near the SPR-active surface and, therefore, changes upon adsorption. For example, when biomolecules in solution bind to receptor molecules immobilized on a region of the gold sensor surface, the corresponding SPR curve minimum typically shifts to larger angles since the refractive index of biomolecules is higher than that of the buffer solutions used. In one method for quantifying SPR spectroscopy data, the full SPR curve (intensity versus incident angle) measured after adsorption for a given region on the surface can be fitted to a bilayer model with the Fresnel equations to determine both the average thickness (within the probed area) and refractive index of the adsorbed film.<sup>11,24,25</sup> Such adsorbed films typically contain both adsorbate molecules and, between them, buffer solution, and so they show a refractive index that is a volume average of the adsorbate and the buffer.<sup>26</sup> If the refractive indices of both the adsorbate and buffer are known, the fraction of this adsorbed film's volume that is adsorbate is then obvious. Multiplying this by the film's thickness provides the volume of adsorbate molecules per unit area and, if the

adsorbate's density is known, the mass of adsorbed molecules per unit area.

Alternatively, the adsorption-induced shift in the SPR minimum angle can be converted directly to the volume of adsorbate per unit area using simple formulas developed by our group for quantitation of SPR spectroscopy data.<sup>26</sup> This method requires a simple calibration of the instrument's response sensitivity (shift in SPR minimum angle per unit change in bulk refractive index), which is constant over the range of changes of importance here. Thereafter, the angle shift due to any adsorption process can be easily converted into an "effective" change in refractive index,  $\Delta n_{\text{eff}}$ , by simply dividing by this sensitivity. We showed in ref 26 (and review again below) how the value of  $\Delta n_{\text{eff}}$  then can be converted to the volume of adsorbate per unit area (i.e., the effective thickness of a pure adsorbate film), provided the refractive index of both the adsorbate and the buffer solution are known. Multiplying this by the density of the pure adsorbate provides the mass of adsorbate per unit area. Alternatively, dividing this by the partial molar volume of the adsorbate in the same buffer provides the number of moles of adsorbate per unit area.<sup>26</sup>

Both of the above methods for quantitative SPR spectroscopy can also be applied to SPR microscopy, but to do so requires measuring the specularly reflected light intensity in a spatially resolved way versus angle while scanning the angle of incidence of the light. The former method has already been applied to quantify SPR microscopy data.<sup>9,16,27</sup> Due to the time it takes to scan the incident/detection angles with an SPR microscope, even slow adsorption events cannot be followed in real time by tracking shifts in the SPR angle with these methods. So, in reality, the above methods are mainly limited to quantifying adsorbate coverage after it has reached some steady-state value in time.

To obtain real-time information about adsorption and desorption kinetics with SPR microscopy, a spatially resolved measurement of reflectivity at a single angle obviously would provide much better time resolution. A few research groups have measured intensity changes at a single angle to qualitatively assess thickness or refractive index changes on an SPR-active surface.<sup>9,12,13,17,18,28</sup> Typically, reflected intensity measurements (i.e., camera images of reflected light intensity versus position on the surface) are used to compare adsorption at differently functionalized areas of a sensor surface at a single time point. Line profiles of SPR microscope images have been used to compare the relative adsorption coverages after saturation at an array of binding sites on a sensor surface.<sup>13,17–19,21,22,28</sup> Time-resolved changes in reflected intensity also have been measured by a few groups.<sup>9,12,16</sup> These groups obtained adsorption and desorption curves by averaging changes in reflected intensity for selected regions of a series of images measured at a single angle, either after the images had been collected<sup>12,16</sup> or during image collection for real-time data acquisition.<sup>9</sup> However, the relationship between reflected light intensity and absolute adsorbate coverage was not addressed.

In this paper, we present a generalized method for converting the change in reflected intensity measured with 1-s time resolution by the SPR microscope at a properly selected "high-contrast" angle into absolute adsorbate coverage or film thickness. We show that, for small changes in the SPR angle, the changes in reflected

(21) Brockman, J. M.; Frutos, A. G.; Corn, R. M. *J. Am. Chem. Soc.* **1999**, *121*, 8044–8051.

(22) Jordan, C. E.; Frutos, A. G.; Thiel, A. J.; Corn, R. M. *Anal. Chem.* **1997**, *69*, 4939–4947.

(23) Shumaker-Parry, J. S.; Aebersold, R.; Campbell, C. T. Submitted to *Anal. Chem.*

(24) Homola, J.; Yee, S. S.; Gauglitz, G. *Sens. Actuators, B* **1999**, *54*, 3–15.

(25) Brockman, J. M.; Nelson, B. P.; Corn, R. M. *Annu. Rev. Phys. Chem.* **2000**, *51*, 41–63.

(26) Jung, L. S.; Campbell, C. T.; Chinowsky, T. M.; Mar, M. N.; Yee, S. S. *Langmuir* **1998**, *14*, 5636–5648.

(27) Hickel, W.; Knoll, W. *J. Appl. Phys.* **1990**, *67*, 3572–3575.

(28) Frey, B. L.; Jordan, C. E.; Kornguth, S.; Corn, R. M. *Anal. Chem.* **1995**, *67*, 4452–4457.

intensity at such a high-contrast angle are proportional to changes in the effective refractive index and effective thickness or surface coverage of an adlayer on an SPR-active surface. We show that this relationship is due to the nearly linear shape of the SPR curve at high contrast angles.

Recently Nelson et al.<sup>19</sup> used theoretical calculations based on Fresnel equations to show that increases in the refractive index in a thin film of fixed thickness (5 nm) near an SPR-active surface results in linear changes in the reflected intensity for an angle in the steep region just below the SPR minimum.<sup>19</sup> They used this proportional relationship to argue that intensity changes measured at this fixed angle by the SPR microscope should be proportional to the relative RNA and DNA surface coverages on an array of immobilized DNAs. They thus modeled this adlayer as being of fixed thickness wherein the refractive index changed proportionally to the amount of added (hybridized) DNA or RNA per unit area.

Here we present a more detailed analysis of the relationship between the changes in reflected intensity at high contrast angles in SPR microscopy and the absolute adsorbate coverage. In doing so, we first derive a relationship between these reflected intensities and changes in the "effective refractive index" ( $\Delta n_{\text{eff}}$ ). We show how this relationship can be used to measure absolute adsorbate coverages versus time with 1-s time resolution and the spatial resolution of the SPR microscope (in principle down to 4  $\mu\text{m}$ ) using a simple calibration of the system's response to bulk refractive index changes.

The framework for SPR microscopy data quantitation presented here is an extension of methods published previously for quantitation of SPR spectroscopy data.<sup>26</sup> We describe in detail the criteria for selection of a single, high-contrast angle in a nearly linear region of a reflected intensity versus angle curve. We show how intensity changes measured at such a properly selected angle are related to the shift in the SPR curve minimum and can be converted to effective refractive index, effective adlayer thickness, and absolute surface coverage of adsorbed molecules, where the linear response error is below  $\sim 9\%$ .

We demonstrate the applications of this quantitation method to time and spatially resolved measurements of absolute coverages made with a home-built SPR microscope during protein adsorption onto gold and onto protein/DNA arrays on gold. For simultaneous measurement of adsorption in all 200  $\mu\text{m} \times 200 \mu\text{m}$  spots within a 4 mm  $\times$  6 mm area with 1-s time resolution, we demonstrate a detection limit for the change in effective refractive index of  $\sim 1.9 \times 10^{-5}$ , or 1.2 ng/cm<sup>2</sup> of protein (0.5 pg in each spot) and a dynamic range of  $\sim 720$  ng/cm<sup>2</sup> of adsorbed protein ( $\sim 4$  close-packed monolayers, for a protein such as BSA). Elsewhere, we have applied this same method to quantitatively measure protein adsorption to sequence-specific binding sites in surface-immobilized double-stranded DNA patterned as an array onto an SPR-active surface with spatial resolution that allows separate but simultaneous determination of absolute protein coverage with 1-s time resolution on each 200- $\mu\text{m}$  element of the array.<sup>23</sup>

## EXPERIMENTAL SECTION

**SPR Microscope.** Our home-built SPR microscope is described in detail elsewhere.<sup>29</sup> Briefly, a stabilized 632.8-nm HeNe

laser serves as the excitation source for the system. Its long-term intensity is specified to be stable to  $<0.2\%$ . The laser beam is p-polarized, expanded and collimated before traveling through an SF14 glass hemicylindrical prism (R. Mathews Optical Works, Inc., Poulsbo, WA) and substrate (25  $\times$  35  $\times$  3 mm SF14 glass slide, Schott Glass Technology, Durea, PA) to illuminate an  $\sim 24\text{-mm}^2$  area of this gold-coated sensor surface. The reflected light is focused and directed by a lens directly onto the CCD detector of a video camera, creating an image that is automatically digitized by a framegrabber card (DT3155, Data Translation, Marlboro, MA) and stored using image acquisition software (KSA400, k-Space Associates, Inc., Ann Arbor, MI). The detection optics are connected to an aluminum rail that is attached to a motorized rotation stage. This stage is mounted under an identical stage that holds the prism. The centers of rotation for the two stages are aligned. A computer connected to a stage controller/driver is used to separately and equally vary the angle of incidence and the angle of detection so the CCD detector stays at the specular angle for each angle of incidence. A neutral density filter decreases the laser power to prevent flooding of the CCD camera. The entire system is mounted on a laser table and covered by a black box to minimize stray light, dust, and air flow effects.

The image acquisition software controls the CCD camera exposure time, frame averaging, and conversion of measured light intensity values to gray scale levels. A key feature of the software is its ability to integrate the intensity in any number of selected regions of an image simultaneously and plot/store that region's integrated intensity versus time in real time.

The fluidics system includes a low-volume ( $\sim 15\text{-}\mu\text{L}$ ) flow cell, a syringe pump, two switching valves, and low dead-volume laminar flow tubing. The syringe is computer controlled using existing software for rapid time response ( $\sim 1$  s).

**Sensor Preparation.** SPR microscope substrates were coated and cleaned according to the procedures described previously.<sup>26</sup> Briefly, SF14 glass slides (substrates) were coated with gold ( $\sim 50$  nm) and cleaned with basic peroxide solution, rinsed copiously with 18 M $\Omega$  water and absolute ethanol, and dried with a stream of nitrogen. Index match fluid (Cargille Laboratories, Inc.) was applied to the back of the substrate before mounting the substrate on the prism for experiments.

**Calibration Solutions.** A series of calibration solutions with concentrations ranging from 0.5 to 70.0 mass % absolute ethanol in water were prepared. The refractive index of the solutions was measured using an Abbe-3L refractometer (Milton Roy Co., Rochester, NY). Measured values were verified with published data.<sup>30</sup> We chose to use ethanol due to its low surface activity and good ability to mix with water. The refractive index of the solutions encompassed the range we plan to monitor in our adsorption experiments.

**Buffer and Protein Solutions.** Streptavidin (SA) and bovine serum albumin (BSA) fraction V were purchased from Calbiochem (San Diego, CA) and Sigma, respectively. These proteins were used without further purification. For BSA adsorption experiments, the carrier buffer was 100 mM PBS, 120 mM NaCl, pH 7.4. BSA solutions were prepared as 1 mg/mL BSA in the carrier buffer.

(29) Shumaker-Parry, J. S.; Nelson, K. E.; Campbell, C. T. In preparation.

(30) *CRC Handbook of Chemistry and Physics*, 81st ed.; CRC Press: Cleveland, OH, 2001.

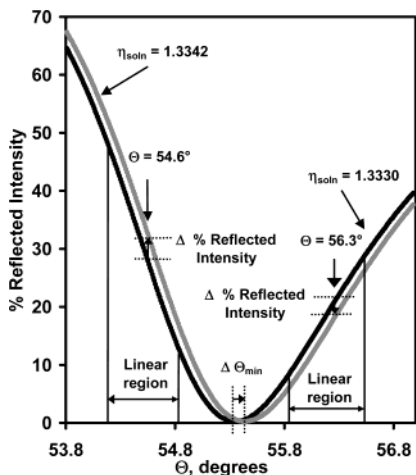


Figure 1. SPR reflectivity curves predicted from Fresnel calculations. A dielectric stack model was used to calculate the responses for infinitely thick layers of refractive indices 1.3330 (black circles) and 1.3342 (gray circles) in contact with a 47.5-nm-thick gold film on an SF14 prism illuminated by 632.8-nm wavelength light.

SA solution was prepared at a concentration of 0.06 mg/mL in 150 mM PBS buffer at pH 7.4 for SA adsorption experiments.

## RESULTS AND DISCUSSION

**Prediction of Reflected Light Intensity Changes from Calculated SPR Curves.** The reflectivity curves in Figure 1 were calculated using a thin-film model based on Fresnel calculations by Hansen.<sup>31</sup> The model is a dielectric stack consisting of an infinitely thick layer of solution with fixed refractive index in contact with a 47.5-nm-thick gold film on an SF14 prism illuminated by 632.8-nm wavelength light. The program used for the calculations was written and made available on-line by Professor Robert Corn's research group.<sup>32</sup> The curves shown correspond to the response from two bulk solutions whose refractive indices are 1.3330 (black circles) and 1.3342 (gray circles), a difference of 0.0012.

Both curves in Figure 1 show the characteristic dip in reflected intensity due to resonance between the incident light and the surface plasmons propagating at the surface/dielectric interface. The minimum shifts to greater angle when the solution's refractive index increases. The vertical black lines in Figure 1 indicate the angle ranges over which there are broad, nearly linear regions on either side of this minimum where the magnitude of the slope (intensity versus angle) is nearly constant near its maximum value. In the discussion below, we will refer to these ranges where the slope is large and remains constant ( $\pm 9\%$ ) as "linear regions" or "high-contrast angles". The left-hand range, for example, extends from  $54.18^\circ$  to  $54.80^\circ$  for the curve corresponding to a bulk refractive index of 1.3330. When the SPR curve moves to higher angles due to the refractive index increase, there is a shift in the measured reflected light intensity in both linear regions as shown by the arrows. If the incident/detection angles are set to an angle in the linear region on the left side of the curve's minimum (e.g.,  $54.6^\circ$ ), an increase in reflected light intensity is observed as the minimum shifts to higher angles. If the reflected light intensity is

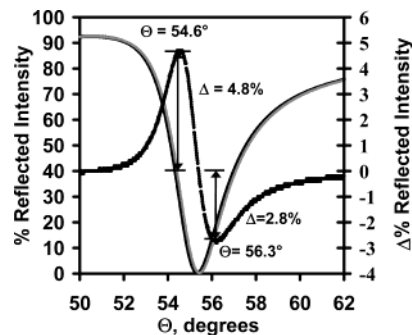


Figure 2. Calculated SPR reflectivity curves (black line  $\eta = 1.3330$  and gray line  $\eta = 1.3342$ ) and the resulting difference curve (black circles) plotted on an expanded scale. The reflectivity curves are the curves from Figure 1 plotted for a larger angle range. The difference curve for the reflectivity curves shows the magnitude of the light intensity shifts due to the increase in refractive index of the layer adjacent to the gold surface in the model used for calculations (right axis).

monitored at an angle in the linear region on the right side of the curve's minimum (e.g.,  $56.3^\circ$ ), the measured reflected intensity decreases.

The SPR curves from Figure 1 are replotted for a larger angle range in Figure 2. The difference curve plotted on an expanded scale shows the magnitude of the change in reflected light intensity when the SPR curve shifts to greater angles due to the increase in refractive index of the layer adjacent to the gold surface. (The percentages plotted here refer to absolute reflectivity, not the original reflectivity at each angle.) The refractive index shift of 0.0012 or 0.09% produces an intensity increase at  $54.6^\circ$  of 4.8% and an intensity decrease at  $56.3^\circ$  of 2.8%, again in absolute reflectivity units, not relative.

Similar difference curves (relative to a refractive index of 1.3330) were calculated for a series of solutions with increasing bulk indices of refraction. Angles from the linear regions of the SPR curve (for a refractive index of 1.3330) in Figure 1 were selected and used to find the corresponding reflected intensity changes from these difference curves.

The absolute value of the change in measured reflected intensity versus the change in bulk refractive index for two fixed, high-contrast angles (selected from both sides of the SPR reflectivity versus angle curve) are plotted in Figure 3. The relationship is linear for intensity changes of less than 20% and 10% for high-contrast angles below and above the SPR resonance, respectively. The initial linear relationship is a natural consequence of the linear shape of the SPR curve at these angles as highlighted by the solid black lines in Figure 1.

Both curves in Figure 3 become nonlinear for larger refractive index changes. At  $54.6^\circ$  (left side), the intensity eventually saturates as expected due to the saturation of intensity as one moves left on the SPR intensity/angle curve of Figure 2. At  $56.1^\circ$  (right side), the absolute value of the intensity change (negative here) saturates and then decreases in Figure 3, as expected as one moves from right to left in the SPR intensity/angle curve of Figure 2, passing through the minimum.

**Measurement of Changes in Reflected Intensity versus Bulk Refractive Index Change.** The predicted SPR curves above show that, when the SPR response is measured as the intensity change at a fixed angle, it too is directly proportional to the change

(31) Hansen, W. N. *J. Opt. Soc. Am.* **1968**, *58*, 380–390.

(32) Corn, R. M.; <http://corninfo.chem.wisc.edu/calculations.html>.

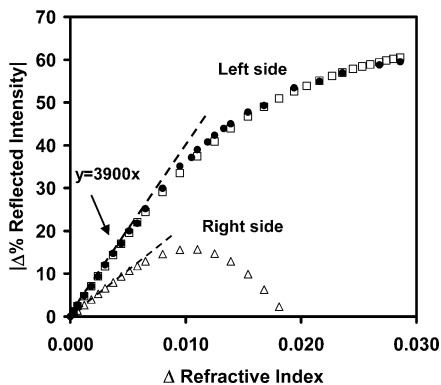


Figure 3. Calculated (open symbols) and measured (filled circles) relationship between absolute changes in reflected intensity and changes in bulk refractive index at angles in the nearly linear regions on the left and right sides of the SPR reflectivity curve minimum. The calculated changes are for incident angles of  $54.6^\circ$  ( $\square$ ) and  $56.1^\circ$  ( $\triangle$ ) on the left and right sides, respectively. The experimental changes are at an angle of  $54.08^\circ$  on the left side of the SPR minimum in Figure 4. The measured curve ( $\bullet$ ) and the curve predicted from the Fresnel equations agree well.

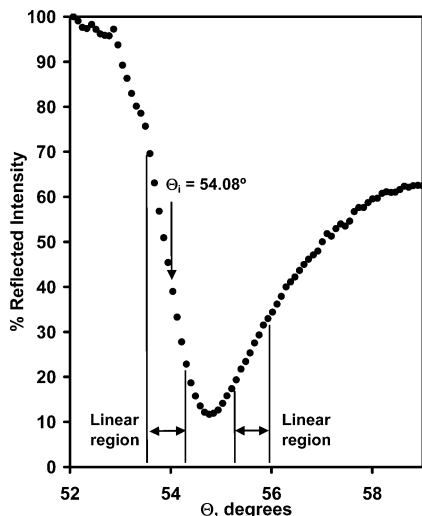


Figure 4. SPR reflectivity curve measured for a gold-coated substrate in contact with pure water using the SPR microscope.

in bulk refractive index near the sensing surface. We have used single angle measurements to determine the proportionality factor that relates the reflected intensity change to the change in refractive index. To do this, SPR intensity versus angle curves were first collected by measuring the reflected light intensity from different regions of an SPR-active surface using a CCD camera while the incident/detection angles were scanned. Software was used to select several 12 pixel by 18 pixel ( $200\ \mu\text{m} \times 200\ \mu\text{m}$ ) areas of the images that each correspond to a  $0.04\text{-mm}^2$  area of the sensor surface. The intensity in each such region was area-averaged and time-integrated for 1 s (at 30 frames/s).

The SPR reflected intensity versus angle curve in Figure 4 is for one such area on a gold-coated substrate in contact with pure water, but is typical of all areas. Similar to the theoretical SPR curves in Figure 1, there are two linear regions, one on each side of the SPR resonance angle.

To measure reflected light intensity shifts versus bulk refractive index, a high-contrast incident angle of  $50.08^\circ$  in the linear region on the left side of the SPR curve minimum was used. The reflected

intensity shifts at this angle for the selected areas were monitored upon introducing a series of ethanol/water solutions into the flow cell in contact with the gold sensor surface. A series of calibration solutions with increasing ethanol concentration added to pure water were introduced, thus varying the refractive index from 1.3330 to 1.3469.

The resulting plot of the reflected intensity change versus change in refractive index is shown in Figure 3 and agrees well with the theoretical plot there. Again, software was used here to integrate the reflected light intensity collected by the CCD camera from each selected  $200\ \mu\text{m} \times 200\ \mu\text{m}$  area and for 1 s. The experimental curve, which is for only one typical area, shows a linear increase in the reflected light intensity for bulk refractive index changes of less than 0.005, similar to the linear range of the calculated curve. The slopes of the linear regions for the two curves are nearly identical: 3900% reflected intensity/RIU, where RIU is used here to represent one refractive index unit. (While refractive index is really a unitless quantity, keeping track of these units makes the presentation here easier to understand.) We next show how this slope can be treated as a sensitivity factor for the SPR microscope and can be used to convert intensity changes at high-contrast angles to effective adlayer thicknesses or absolute surface coverages of adsorbed molecules.

**Relationship between Changes in Reflected Light Intensity and Angle Shifts.** As shown above, the intensity change ( $\Delta I$ ) measured at a high-contrast angle (i.e., one in a steep, linear region of the SPR curve) is directly proportional to the change in the bulk refractive index of the solution near the sensor surface, for small changes:

$$\Delta I = s(\Delta\eta) = s(\eta_{\text{initial}} - \eta_{\text{final}}) \quad (1)$$

where  $\eta$  is the refractive index of the solution in contact with the sensor surface and  $s$  is the proportionality constant.

This proportionality is not surprising, since Jung et al. showed a similar proportional relationship between the shift in the SPR resonance angle (at fixed wavelength) or wavelength (at fixed angle) and the bulk refractive index change.<sup>26</sup> Over a narrow refractive index range and in the absence of absorption, they showed that

$$\Delta\Theta_{\text{min}} = m(\Delta\eta) = m(\eta_{\text{initial}} - \eta_{\text{final}}) \quad (2)$$

where  $\Delta\Theta_{\text{min}}$  is the measured SPR resonance angle shift and  $\eta$  is the refractive index of the solution near the sensor surface. Jung et al. described  $m$ , the slope, as a sensitivity factor for SPR spectroscopy systems, which can be determined easily by a calibration plot of  $\Delta\Theta_{\text{min}}$  versus bulk refractive index. As shown diagrammatically in Figure 1, for a linear region of a typical SPR curve with slope  $M$  (percent reflected intensity per degree), a differential shift in the SPR minimum angle  $\Theta_{\text{min}}$  by  $d\Theta_{\text{min}}$  will cause a proportional differential change in percent reflected light intensity at a given high-contrast angle  $\Theta_i$ , given by

$$dI = M d\Theta_{\text{min}} \quad (3)$$

For a finite range of change in  $\Theta_{\text{min}}$  this integrates into

$$\Delta I = M\Delta\Theta_{\min} \quad (4)$$

Combining eqs 2 and 4 gives

$$\Delta I = Mm\Delta\eta = s\Delta\eta \quad (5)$$

the same proportional relationship as eq 1, with  $s = Mm$ . The slope,  $s$ , can be considered the sensitivity factor for SPR microscope systems, determined easily by a calibration plot of  $\Delta I$  versus bulk refractive index.

**Prediction of the SPR Microscope's Intensity Response to Thin-Film Adsorption.** Next, we use this proportionality to derive a simple relationship between the measured intensity change in SPR microscopy due to adsorption from liquid solution onto the sensor surface and the adsorbate's film thickness or coverage (mass per unit area). Jung et al.<sup>26</sup> showed that, in SPR spectroscopy, the change in the SPR minimum angle due to adsorption is given by

$$\Delta\Theta_{\min} = m\Delta\eta_{\text{eff}} \quad (6)$$

where  $m$  is the slope of the calibration plot (see eq 2) used to find an SPR spectrometer's sensitivity factor and  $\eta_{\text{eff}}$  is the "effective" refractive index of the material in contact with the SPR-active metal surface. Note that  $\eta_{\text{eff}}$  is the properly weighted average of the refractive index of any adsorbed layers plus the bulk solution, which reflects in an accurate way the surface sensitivity of the SPR measurement (which decays exponentially away from the metal surface). It was proven that  $\eta_{\text{eff}}$  is, to a very close approximation, given by<sup>26</sup>

$$\eta_{\text{eff}} = (2/l_d) \int_0^{\infty} \eta(z) \exp(-2z/l_d) dz \quad (7.1)$$

where  $\eta(z)$  is the area-averaged index of refraction at distance  $z$  from the metal and  $l_d$  is the decay length of the evanescent field near the gold surface. (Note that  $l_d/2$  is the decay length of this evanescent light's intensity, which determines the probe depth of SPR technique.) The value for  $l_d$  typically is  $37 \pm 13\%$  of the wavelength of the light and can be calculated more accurately using Maxwell's equations from<sup>26</sup>

$$\begin{aligned} l_d &= (\lambda/2\pi) / \text{Re}\{[\eta_{\text{eff}}^2 \epsilon_{\text{metal}} / (\eta_{\text{eff}}^2 + \epsilon_{\text{metal}})] - \eta_{\text{eff}}^2\}^{1/2} \\ &= (\lambda/2) / \text{Re}\{-\eta_{\text{eff}}^4 / (\eta_{\text{eff}}^2 + \epsilon_{\text{metal}})\}^{1/2} \end{aligned} \quad (7.2)$$

where  $\epsilon_{\text{metal}}$  is the complex dielectric constant of the metal at the wavelength of the measurement (tabulated elsewhere<sup>33,34</sup>) and  $\eta_{\text{eff}}$  is the effective index of refraction of the sample in question.

Substituting eq 6 into eq 4 gives

$$\Delta I = Mm\Delta\eta_{\text{eff}} = s\Delta\eta_{\text{eff}} \quad (8)$$

where  $s = Mm$ . Note that  $s$  is the slope of the calibration plot of  $\Delta I$  versus  $\Delta\eta_{\text{eff}}$  measured by monitoring the instrument's response

(reflected light intensity at a high-contrast angle) to changes in bulk refractive index (when adsorption is negligible), exactly as done in Figure 3. Thus, measuring  $\Delta I$  allows a direct measurement of  $\Delta\eta_{\text{eff}} = \Delta I/s$ .

When  $\Delta\eta_{\text{eff}}$  is measured in the case of some adsorbate adsorbing onto the surface, one can use its value to determine the adsorbate's effective film thickness and absolute coverage ( $\text{g}/\text{cm}^2$ ) on the surface following exactly the same procedures as outlined in ref 26. Substituting into eq 8 the expression in eq 7 for  $\eta_{\text{eff}}$  gives

$$\Delta\eta_{\text{eff}} = \Delta I/s = (2/l_d) \int_0^{\infty} \Delta\eta(z) \exp(-2z/l_d) dz \quad (9.1)$$

where  $\Delta I$  is the measured reflected intensity shift at a high-contrast angle,  $\Delta\eta(z)$  is the change in the area-averaged refractive index at distance  $z$  from the surface, and  $s$  is the SPR microscope sensitivity factor. For the special case that  $\Delta I$  is measured between an initial time with the surface in solution of refractive index  $\eta_s$  and no adsorbate and a final time with an adsorbed film of thickness  $d$  (much less than  $l_d$ ) and refractive index  $\eta_a$ , then this integral simplifies (as shown in ref 26) to give

$$\Delta\eta_{\text{eff}} = \Delta I/s = (2d/l_d)(\eta_a - \eta_s) \quad (9.2)$$

**Estimation of Adlayer Thickness and Surface Coverage from Intensity Changes.** Solving eq 9.2 for the effective thickness gives

$$d = \left(\frac{l_d}{2}\right) \left[ \frac{\Delta I}{s(\eta_a - \eta_s)} \right] \quad (10)$$

The value for  $l_d$  needed here should be calculated from eq 7.2, using the value for  $\eta_{\text{eff}}$  determined experimentally by comparing the observed SPR intensity change to a calibration curve of change in SPR intensity versus change in bulk refractive index like Figure 3. Equation 10 also applies whenever the adsorbate binds to a surface that was precoated with another film (for example, containing receptors that specifically recognize and bind the adsorbate of interest).<sup>26</sup> When the adsorbate film is rough or porous (e.g., interspersed with solvent), this thickness  $d$  refers to the "effective thickness", i.e., the thickness that same number of adsorbate molecules per unit area would have if adsorbed in a flat film of uniform thickness of pure adsorbate at the same density for which the value  $\eta_a$  refers.<sup>26</sup> The *absolute* accuracy of this approach for measuring absolute thicknesses with SPR spectroscopy was shown to be better than  $\pm 35\%$  with, of course, a much better precision.<sup>26</sup> The accuracy is typically limited by the accuracy of the parameter  $\eta_a$ , which often is only known approximately. It follows from the above derivation that these same statements apply also to the use of eq 10 for quantifying adsorbate thicknesses with SPR microscopy data.

Once the effective thickness of the adsorbed layer is found, it is simple to estimate the surface coverage of adsorbed molecules. Multiplying  $d$  by the density of the pure adsorbate provides the mass of adsorbate per unit area. The surface coverage also may

(33) Innes, R. A.; Sambles, J. R. *J. Phys. F: Met. Phys.* **1987**, *17*, 277-287.

(34) *Handbook of Optical Constants of Solids*; Academic Press: Orlando, FL, 1985.

be calculated from the bulk number density,  $N$ , and the thickness found in eq 10 using

$$\text{coverage (molecules/cm}^2\text{)} = d \text{ (cm)} \times N \text{ (molecules/cm}^3\text{)} \quad (11)$$

The bulk number density,  $N$ , can be estimated by dividing the bulk density for the pure condensed adsorbed material by the molecular weight and multiplying by Avogadro's number.

To calculate an adlayer thickness, the refractive index of the adsorbate and the solution must be known. The refractive index of the solution may be measured using a standard Abbe refractometer as was done for the calibration solutions. The value used for  $n_a$  (the refraction index) and density (or  $N$ ) of the molecule in pure condensed form can usually be found in the literature or measured. For molecules such as proteins and DNA that cannot be obtained in pure form or that have quite different charge distribution when in solution, it is better to estimate its refractive index from the contribution they make to the refractive index of a bulk solution as described in detail by Jung et al.<sup>26</sup> In such cases, dividing  $d$  by the partial molar volume of the adsorbate in the same buffer provides the number of moles of adsorbate per unit area.<sup>26</sup>

**Inaccuracies Due to Changes in SPR Line Shape and Their Approximate Correction.** The above equations assume that the SPR curve line shape does not change with the small increases in  $\eta_{\text{eff}}$  that accompany adsorption. Actually, the SPR line shape (reflected intensity versus angle) broadens slightly with increasing bulk refractive index and broadens slightly more if the same change in  $\eta_{\text{eff}}$  is induced by the adsorption of a thin film of molecules with a high refractive index, like proteins. However, the extent of broadening is very small in the range of changes of  $\eta_{\text{eff}}$  where we propose that the above equations be applied (increases in  $\eta_{\text{eff}}$  up to 0.011 RIU, corresponding to  $\sim 4$  monolayers of a typical protein; see below). The important measure of the extent of this broadening is the decrease in the value of the slope  $M$  of the linear region of the SPR curve (percent reflected intensity per degree; see Figure 1). Fresnel calculations such as in Figures 1–3 proved that this absolute magnitude of the slope decreases by only 4% for the maximum bulk refractive index increase of 0.011 RIU in this range and by  $<10\%$  when this same change in  $\eta_{\text{eff}}$  is induced by the adsorption of protein. (These relative changes in slope are the same on the left and right sides of the SPR curve.) These decreases in slope mean that the increase in reflected intensity at any given high-contrast angle are slightly less than predicted by the above equations. This also means that the change in effective refractive index or an adsorbate's film thickness or coverage estimated from the measured intensity changes using the above equations will be slightly too high.

Typically, the way a quantitative measurement of adsorption amount is done using the above equations is to measure the slope  $s$  of the calibration plot (intensity versus bulk refractive index), as in Figure 3. This slope, taken at the average value of  $\eta_{\text{eff}}$  over the range being probed, is then used in the equation  $\Delta\eta_{\text{eff}} = \Delta I / s$  to calculate a value of  $\Delta\eta_{\text{eff}}$  from the measured change in intensity ( $\Delta I$ ) for an adsorption experiment (see eq 8). Then,  $s$  and  $\Delta I$  are used in eqs 10 and 11 to estimate a film thickness and coverage. Fresnel calculations prove that the decrease in  $s$

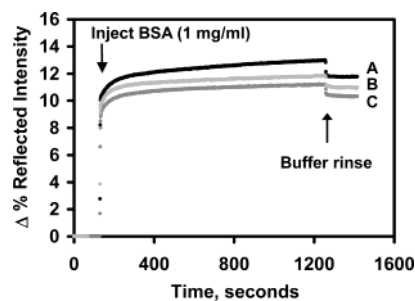


Figure 5. BSA adsorption from aqueous buffer at three spatially separated areas (A–C), each of  $200 \mu\text{m} \times 200 \mu\text{m}$ , on a gold-coated substrate measured using the SPR microscope. Adsorption was monitored by integrating the light intensity for the selected regions of the SPR microscope image. The baseline was established by introducing carrier buffer into the flow cell. Then, BSA in carrier buffer was injected. As the BSA adsorption approached saturation coverage, the protein sample was replaced with carrier buffer.

mentioned above leads to slight overestimates in  $\Delta\eta_{\text{eff}}$ , film thickness, and coverage, but this error is  $<5\%$  in the usable linear dynamic range we propose below (increases in  $\eta_{\text{eff}}$  up to 0.011 RIU, corresponding to  $\sim 4$  monolayers of a typical protein).

One could improve the accuracy slightly by recognizing that this effect occurs and decrease the film thickness or coverage estimates by  $\sim 1\%$  for every 0.002 RIU change in  $\eta_{\text{eff}}$ . This correction is usually negligible compared to the errors introduced by our inaccurate knowledge of the value of the refractive index of the adsorbate.

**Application of Method to Spatially Resolved Quantitation of Protein Adsorption.** The SPR microscope response was measured for the adsorption of BSA from aqueous buffer solution onto a bare gold-coated substrate. Initially, SPR (reflected intensity versus angle) curves were collected for preselected areas ( $200\text{-}\mu\text{m}$  squares) chosen randomly across the  $24\text{-mm}^2$  illuminated region of the sensor surface. Then, an incident angle was selected which, for all areas of interest, was from the middle right portion of the linear region on the left side of the SPR curves, and the reflected light intensity at this angle was monitored simultaneously in real time for the preselected areas, with 1 s/data point. Three representative response curves from spatially well-separated areas of the sensing surface are shown in Figure 5. After establishing a steady baseline with the carrier buffer, BSA solution (1 mg/mL) in the exact same buffer was injected into the flow cell. After adsorption slowed, the BSA solution was replaced by the carrier buffer. Although the final surface coverages are slightly different, the initial overlap of the three adsorption curves shows the optimization of the fluidics system for simultaneous delivery of sample to all areas of the sensing surface and the fast time response. The curves for regions A–C were selected to show the maximum range in the adsorption response across the surface. The variance may be due to inhomogeneities on the Au surface affecting surface coverages or differences in the sensitivity factor  $s$  due to small deviations in the slope of the SPR curve measured for regions across the sensor surface. (In principle, one could get a slightly different sensitivity for each region as in Figure 3.)

For 12 similar areas representative of the probed region of the sensor surface, the saturation response measured for BSA adsorption was  $11.4 \pm 0.7\%$  reflected intensity change. This can be converted to an effective film thickness using eq 10. The

sensitivity factor was measured (Figure 3) to be 3900% reflected intensity/RIU. The value for  $\eta_a$  for BSA was estimated to be 1.57, the refractive index for this class of proteins.<sup>26</sup> The value for  $\eta_s$  for the buffer was measured and found to be 1.334. The decay length,  $l_d$ , was calculated with eq 7.2 to be 234 nm for the excitation wavelength used.<sup>26</sup> Using these values, an effective thickness of 1.45 nm was calculated for the BSA layer.

Using the specific volume for BSA of  $0.77 \text{ cm}^3/\text{g}$ ,<sup>35–37</sup> this effective thickness of 1.45 nm converts to a saturation surface coverage of  $1.82 \times 10^{-7} \text{ g/cm}^2$ , or  $1.82 \times 10^{12}$  molecules/cm<sup>2</sup>. This is  $\sim 30\%$  less than the calculated close-packed density of  $2.5 \times 10^{-7} \text{ g/cm}^2$  for BSA on a planar surface.<sup>38</sup> However, it is within 7% of the BSA saturation coverage on bare gold measured by Jung et al. using SPR spectroscopy.<sup>26</sup> From that SPR system's response, a protein surface coverage of  $1.71 \times 10^{-7} \text{ g/cm}^2$  was calculated. Similar saturation surface concentrations of  $(1.2\text{--}2.2) \times 10^{-7} \text{ g/cm}^2$  were measured for BSA adsorption onto several polymer surfaces.<sup>38,39</sup> Alkylthiol SAMs terminated with  $\text{CH}_3$  or  $\text{C}_6\text{H}_5\text{OH}$  groups on gold also adsorbed similar BSA saturation coverages of  $(0.85\text{--}1.1) \times 10^{-7} \text{ g/cm}^2$  as measured by SPR spectroscopy.<sup>40</sup>

Figure 6 shows a SPR microscope image of a  $8 \times 12$  SA + dsDNA array and simultaneous, real-time measurements of the protein SA binding to the array spots and surrounding regions. The dsDNA array was prepared on a biotin-containing mixed self-assembled monolayer (SAM) on a gold-coated substrate using a SA linker layer, with methods similar to those described in detail elsewhere (but not yet optimized).<sup>41</sup> First a SA array was made by using a robotic microspotting device to deliver SA solution in an  $8 \times 12$  array of spots onto a gold surface prefunctionalized with the mixed SAM. Then dsDNA was spotted on top of these SA spots. The top two rows and the bottom row of array spots contain SA without dsDNA. The SA and dsDNA coverages in the spots were quantified by measuring the reflected intensity for a  $200 \mu\text{m} \times 200 \mu\text{m}$  area in the center of each element of the array and in the same size area of the SAM surface located just below each array element. The difference in reflected intensity was calculated by subtracting the intensity for the surrounding SAM surface from that for the array element, and the quantitative methods described above were used to calculate SA and dsDNA packing densities. The average difference in reflected intensity for the SA spots was  $8.3 \pm 0.8\%$ , corresponding to an average SA packing density of  $1.4 \times 10^{12} \text{ SA/cm}^2$ , or 58% of the typical SA saturation coverage reported on this SAM.<sup>43</sup> The difference in reflected intensity in the DNA spots due to the dsDNAs, found by subtracting the average difference in percent reflected intensity for the SA spots from the average difference in percent reflected intensity for the spots containing both SA and DNA, was  $2.4 \pm$

(35) Darnell, J. E.; Lodish, H.; Baltimore, D. *Molecular Cell Biology*; Scientific American Books: New York, 1990.

(36) Leslie, T. E.; Lilley, T. H. *Biopolymers* **1985**, *24*, 695–710.

(37) Sjölander, S.; Urbaniczky, C. *Anal. Chem.* **1991**, *63*, 2338–2345.

(38) Fair, B. D.; Jamieson, A. M. *J. Colloid Interface Sci.* **1980**, *77*, 525–534.

(39) Gölander, C.-G.; Kiss, E. *J. Colloid Interface Sci.* **1987**, *121*, 240–253.

(40) Silin, V.; Weetall, H.; Vanderah, D. J. *J. Colloid Interface Sci.* **1997**, *185*, 94–103.

(41) Shumaker-Parry, J. S.; Zareie, M. H.; Aebersold, R.; Campbell, C. T. *Anal. Chem.* **2004**, *76*, 918–919.

(42) Shumaker-Parry, J. S.; Campbell, C. T.; Stormo, G. D.; Silbaq, F. S.; Aebersold, R. H. *Proc. SPIE-Scanning and Force Microscopies for Biomedical Applications II*; San Jose, CA, 2000; pp 158–166.

(43) Jung, L. S.; Nelson, K. E.; Stayton, P. S.; Campbell, C. T. *Langmuir* **2000**, *16*, 9421–32.

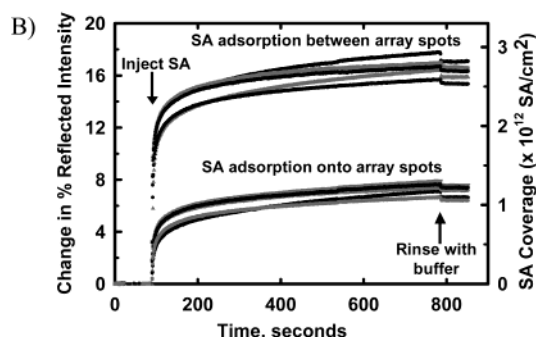
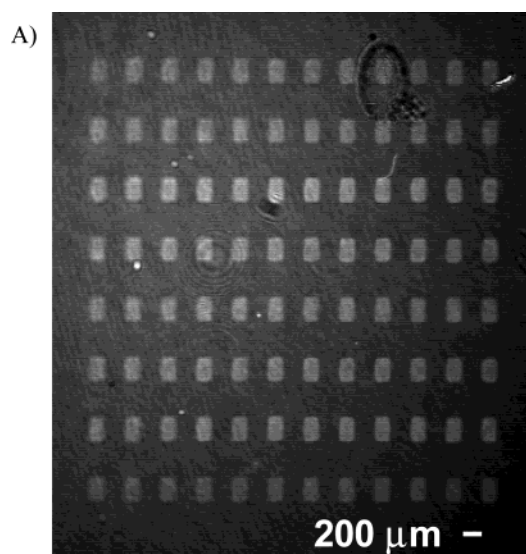


Figure 6. (A) High-contrast-angle SPR microscope image of a SA + dsDNA array under buffer solution and (B) simultaneous, real-time measurements of reflected light intensity from representative areas on the array, showing adsorption and desorption of additional SA. This image and these reflected intensity data are time averages for 1.0 s of video frames and integrated intensity values. (A) The spots in all rows contain SA, and rows 2–7 (from the top) also contain dsDNA. Between the spots is the SAM only. (B) These intensity data were collected by area-integrating the intensity in spatially separated  $200 \mu\text{m} \times 200 \mu\text{m}$  areas on the array surface. Shown are representative curves for five array spots (two containing SA and three containing SA + DNA), and five nearby areas between spots. The baseline was established in PBS buffer. Then SA in solution was introduced to the flow cell (at 100 s). After adsorption approached saturation, pure buffer was injected (at 790 s).

0.8%, which converts to a dsDNA packing density of  $\sim 6 \times 10^{11}$  DNA/cm<sup>2</sup>. These values give a binding ratio of 0.4 dsDNA/SA, which agrees with that found previously for dsDNA immobilized from bulk solution onto a uniform SA monolayer.<sup>42</sup>

After preparing this dsDNA + SA array, it was exposed to a SA solution while monitoring the SPR microscope image versus time, as shown for selected areas in Figure 6B. The measured reflectivity in each spot was converted to added SA surface concentration using the methods described above, as shown on the right axis of Figure 6B. The amount of SA that adsorbs between spots ( $\sim 2.7 \times 10^{12} \text{ SA/cm}^2$ ) is typical of the saturation SA coverage reported on this SAM.<sup>43</sup> The amount of additional SA that binds onto the SA or SA + DNA spots is also consistent with saturation SA binding to this SAM (unaffected by the dsDNA present), given the fact that these spots contained only  $\sim 58\%$

Table 1. Effects of Frame Averaging and Data Collection Duration on the Standard Deviation for Percent Reflected Intensity Measurements

no. of frames averaged/ data point	data points/s	standard deviation (% reflected intensity) for data collected for the duration shown			
		60 s	300 s	600 s	1200 s
1	15	0.0546	0.0553	0.0601	0.0730
5	3	0.0241	0.0260	0.0392	0.0440
15	1	0.0162	0.0188	0.0182	0.0330
30	0.5	0.0108	0.0128	0.0145	0.0434
60	0.25	0.0083	0.0119	0.0228	0.0412
120	0.125	0.0087	0.0153	0.0196	0.0592
240	0.0625	0.0053	0.0116	0.0278	0.0631

this saturation SA coverage initially. These curves demonstrate the ability to measure adsorption and desorption events simultaneously at many regions of the surface with high sensitivity and fast time resolution (1 s) and convert these results to absolute surface concentrations.

Elsewhere we describe the application of these methods to quantify real-time measurements of sequence-specific binding of the transcription factor Gal4 to similar double-stranded DNA arrays.<sup>23</sup>

**Estimation of the SPR Microscope Detection Limits.** The detection limit of our SPR microscope for measuring intensity changes depends on the system noise and the baseline drift. One advantage of our image acquisition software is the ability to integrate the reflected light intensity for a selected number of pixels, which improves the signal-to-noise ratio. We can choose the number of pixels by drawing a box around the region of interest in an SPR microscope image. All of the data discussed in this section are based on intensity integration in regions that are 12 pixels by 18 pixels, corresponding to  $200\ \mu\text{m} \times 200\ \mu\text{m}$  regions of the sensing surface. The software integrates the intensity measured by the camera for each selected region at a rate of 30 Hz.

In addition to providing integration capabilities, the software also controls frame averaging. The increased sampling reduces the random noise without increasing the overall signal intensity. However, an increase in frame averaging leads to a loss in time resolution. Additionally, our framegrabber uses one frame as a reset prior to collecting the next frame, resulting in half the expected data acquisition rate. Table 1 shows the range in standard deviations when different numbers of frames are averaged for different times without using a reference area to account for system drift. The data were calculated from the scatter in the reflectivity data measured at a high-contrast angle for a sensor surface in contact with pure water for the durations listed in Table 1. Also shown are the number of data points collected per second for the indicated average number of frames when a camera frame capture rate of 30 Hz is used in combination with our framegrabber card that uses every other frame for a reset.

For short time periods, there is a decrease in the standard deviation as the number of frames included in averaging increases. For longer times, the decrease in standard deviation for averaging a higher number of frames is not as significant. The improvement at short time periods may be due to the better short-term intensity stability of the HeNe laser. The response measured for longer

time periods is affected more significantly by drift in the system. The ultimate limit for the SPR microscope without using a reference signal from a nearby area is probably determined by the stability of the laser, which is specified to be better than  $\pm 0.1\%$  for short time periods (e.g., 1 min) and  $\pm 0.2\%$  for longer periods (e.g., 1 h). Our noise measurements show the system stability is 10 times better than those specifications, at least for shorter times, without using a reference. For slow adsorption measurements or when kinetics are not important, the frame averaging can be increased to improve the detection limits as shown in Table 1.

Using Table 1, we can estimate the detection limits of our system without using any reference area to remove common drift effects. We typically average 15 frames to obtain 1 data point/s. A typical standard deviation for short-term measurements (10 min) obtained when 15 frames are averaged is  $\pm 0.018\%$  reflected intensity. Since we can measure a signal equal to 4 times the standard deviation,<sup>44</sup> the detection limit for each data point when we average 15 frames is 0.072% reflected intensity.

A detection limit of the SPR microscope for the adsorption of a uniform layer of protein on the sensor surface can be estimated using this measurable signal (at a 1-s time resolution) of 0.072% reflected intensity and eqs 10 and 11. Using the instrument's sensitivity ( $s$ ) of 3900% reflected intensity per RIU (Figure 3), this corresponds to a detection limit of  $1.85 \times 10^{-5}$  RIU. The detection limit of  $1.85 \times 10^{-5}$  RIU converts to a limit in detected protein thickness of 0.009 nm, using 234 nm for  $l_d$  (see above) and 0.24 for  $\eta_a - \eta_s$  for a typical protein in aqueous buffer (see above). This thickness corresponds to  $1.2\ \text{ng}/\text{cm}^2$  or  $5 \times 10^{-3}$  monolayers for a protein such as BSA and assuming a close-packed monolayer in the area analyzed. Note that all these detection limits refer to each single  $200\ \mu\text{m} \times 200\ \mu\text{m}$  area (measured simultaneously with all such areas in a  $4\ \text{mm} \times 6\ \text{mm}$  illuminated region), without use of any background or drift corrections from nearby areas. It thus corresponds to only 0.3 pg of protein in each spot.

The detection limits discussed above were calculated for changes in the reflected light intensity over a 10-min period. As the duration of the experiment increases, the system drift usually becomes larger, and therefore, the detection limit gets worse. This is shown in Table 1 by the increase in standard deviations calculated for data acquired for longer time periods. The increased standard deviations may be due to temperature changes, long-term laser intensity instability, or other drift often observed when using a bare gold sensor for making measurements.

One advantage of SPR microscopy over SPR spectroscopy is that multiple regions on the sensing surface can be monitored simultaneously and used to subtract out common drift and background (by using the signal from a nearby area as a reference) and thus improve detection limits. Table 2 shows how using a reference improves the standard deviation when there is drift. The extent of the drift in the reflectivity used to calculate the standard deviations in the table was larger than usual, resulting in higher standard deviations, even when averaging a large number of frames. The drift is most likely due to temperature changes and laser intensity fluctuations. We also often observe more drift when measuring the SPR response at a bare gold sensor surface (compared to the response for sensor surfaces coated with

(44) Skoog, D. A.; Leary, J. J. *Principles of Instrumental Analysis*; Saunders College Publishing: New York, 1992.

Table 2. Affect of Referencing on the Standard Deviation in the Reflectivity Data Measured Using the SPR Microscope

no. of frames averaged/ data point	data points/s	standard deviation (% reflected intensity)	
		no referencing <sup>a</sup>	referencing <sup>b</sup>
5	3	0.0233	0.0208
15	1	0.0288	0.0201
30	0.5	0.0267	0.0145
60	0.25	0.0264	0.0155
120	0.125	0.0229	0.0154

<sup>a</sup> Standard deviations were averaged for four closely spaced  $200 \mu\text{m} \times 200 \mu\text{m}$  regions on the sensor surface while the surface was in contact with pure water for 300 s. <sup>b</sup> For each region, a nearby region was used as a reference. This was done by subtracting the response for the reference region from the response for the original region. The standard deviation was then calculated for the data after referencing. This process was repeated for each region and the resulting standard deviations were averaged.

a layer of protein such as streptavidin). As shown in Table 2, the use of a reference improves the standard deviations. For longer duration measurements and when the drift is larger, we have observed even greater improvements in the standard deviation when using a reference (e.g., better than a factor of 6; data not shown). The improvement of the detection limit for these measurements highlights the advantages of using a reference channel to account for drift, which is very important when measuring slow adsorption processes, especially if the measured response is close to the detection limit for the system.

The dynamic range of the SPR microscope was estimated using Figure 3. The SPR microscope response is nearly linear for reflectivity shifts of less than 20%. This upper limit for the linear response range corresponds to a bulk refractive index change of 0.0058 and a thickness of 2.9 nm when using the same values in eq 10 as measured and used to calculate the detection limit above. The thickness can be converted to a surface coverage of  $380 \text{ ng/cm}^2$  or 2.1 saturation monolayers of the protein BSA. For "protein chips", this is an acceptable range. In the next section, we show that this range can be doubled to 4 monolayers by optimum selection of the incident angle for adsorption measurements. Because the width and shape of the SPR curve limits the refractive index change range over which a linear response is seen, it may be necessary to adjust the incident angle for each layer when measuring the adsorption of many layers on the same sensor surface, thus effectively extending this dynamic range. In contrast, our SPR spectroscopy system described in ref 26 has a much greater dynamic range ( $\sim 10^{-2}$  to  $>200 \text{ nm}$  in average film thickness) without adjustment because it automatically tracks the shift in the SPR curve minimum.

**Optimum Angle for Intensity Shift Measurements.** Figure 7 shows how the choice of the incident angle affects the sensitivity factor and the dynamic range of the measurement. The change in intensity versus the change in refractive index is shown in Figure 7 for three angles that span the linear region of the left side of the SPR curve minimum in Figure 1. For refractive index changes less than 0.0025, the slope is similar for all three angles ( $3576 \pm 332\%$  reflected intensity/RIU). This demonstrates that the error due to any nonlinearity in the selected linear region will be small ( $<9\%$ ).

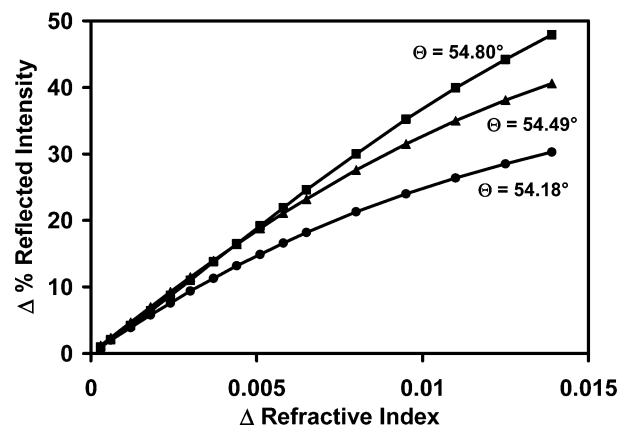


Figure 7. Changes in reflected intensity versus changes in refractive index plotted for angles spanning the linear range on the left side of the SPR curve in Figure 1. The plot was made by applying the same procedures used to obtain the calculated curves in Figure 3. The slight variation in the linear regions of the curves shows the dependence of the sensitivity factor and the dynamic range on the selection of the high-contrast angle.

The choice of angle becomes more important when looking at the variation in the dynamic range across the linear region. The response becomes nonlinear for refractive index changes greater than 0.0025 for an angle of  $54.18^\circ$ . A smaller dynamic range would be expected for this angle because of its position along the linear region of the SPR curve. On the other hand, using the high-contrast angle close to the SPR minimum ( $54.80^\circ$ ) gives a linear response out to  $\sim 0.011 \text{ RIU}$ , twice the range estimated in the previous section. Clearly this is a better choice and corresponds to protein detection with linear response up to  $\sim 720 \text{ ng/cm}^2$  or 4 monolayers.

When selecting the incident angle,  $\Theta_i$ , for adsorption measurements, it is necessary to look at SPR curves collected from different regions of the sensing surface. This is especially important when the surface is functionalized to create an array of binding sites. The incident angle must be selected so all measured reflected intensity changes are in the linear response regime for the SPR microscope. This means the incident angle for an area of the sensor surface must be in the linear region of the corresponding SPR curve for all areas sampled and preferably in the linear region closest to the SPR minimum for all areas. Depending on the functionalization process, the SPR curves may be shifted relative to each other to reflect differences in the local refractive index. This may be due to different packing densities of adsorbed molecules. Typically, arraying techniques are optimized to produce arrays of binding sites with similar packing densities of the immobilized molecule. SPR curves also may be shifted when different types of molecules are immobilized on the same sensing surface. Usually an array is composed of the same class of molecules (e.g., DNAs or proteins), making this easy.

## CONCLUSIONS

We have outlined methods for converting reflected light intensity changes measured by SPR microscopy at a "high-contrast" angle to effective refractive index changes, effective adlayer thicknesses, and adsorbate surface coverages. Thus, real-time intensity changes measured with a video camera are converted to local adsorbate coverages using a sensitivity factor

for the SPR microscope found by a simple calibration measuring the changes in intensity due to changes in bulk refractive index. The detection limit ( $<0.5$  pg of protein per  $200\ \mu\text{m}$  spot at 1-s time resolution) and dynamic range ( $\sim 4$  monolayers of protein) are found for our home-built SPR microscope system, which uses a HeNe laser as the light source. The same type of analysis described here can be applied to systems with different metal coatings (e.g., silver) or different light sources for the SPR sensing.

#### ACKNOWLEDGMENT

This work was made possible by funding from the Institute for Systems Biology and the National Science Foundation.

J.S.S.-P. thanks the University of Washington Center for Nanotechnology and its NSF IGERT program for support in the form of a graduate fellowship. We thank Dr. Ruedi Aebersold, Dr. Leroy Hood, Prof. Rob Corn, Prof. Wolfgang Knoll, and Isabel Alves for helpful and enjoyable discussions. We thank the staff of the Chemistry Department's machine shop and electronics shop for their generous advice and technical assistance.

Received for review August 17, 2003. Accepted November 12, 2003.

AC034962A